Batteries & Supercaps

Perspective
doi.org/10.1002/batt.202500469

Chemistry Europe
European Chemical Societies Publishing

www.batteries-supercaps.org

Fluorine-Free Lithium-Ion Batteries: A Working Alternative

Mark Weijers, Pranav Karanth, Joep Borninkhof, and Fokko M. Mulder*

Current commercial battery designs contain fluorinated materials as binders and electrolyte salts to ensure high electrochemical and thermal stability. Upcoming regulations in Europe and the US restrict the manufacturing of such materials, as their persistence in drinking water and soil can cause long-term ecological harm. In this perspective, a completely fluorine-free battery design that has similar performance compared to commercial standards, while using aqueously processed $LiNi_{0.8}Mn_{0.1}Co_{0.1}O_2$ (NMC811) and graphite as cathode and anode active materials, respectively, is showcased. The cell shows 98% retained capacity after 600 cycles at room temperature, indicating good stability of active material with nonfluorinated binders. The charge rate performance (69% retained capacity at 1C, 1.5 mAh cm^{-2}) can be improved by combining two fluorine-free salts (67% retained capacity at 1C with 2.5 times the loading, 3.3 mAh cm^{-2}). This work illustrates that fluorine-free cell designs show good battery performance over a wide potential window.

1. Introduction: The Need for Fluorine-Free Lithium-Ion Batteries

Current commercial battery designs contain highly fluorinated molecules to ensure high electrochemical and thermal stability. Binders, such as polyvinylene difluoride (PVDF), polytetrafluorethylene, electrolytes containing lithium salts in the form of lithium hexafluorophosphate ($LiPF_6$), and additives like fluoroethylene carbonate, have become the state-of-the-art in cathode and electrolyte manufacturing, respectively.[1–4] The beneficial (electro) chemical stability features of these materials when confined inside a battery cell are, however, proving to be harmful outside of their application area, i.e., during manufacturing, recycling, and end-of-life demolition. Fluorinated alkanes and HF-producing substances are indicated to be harmful, as they induce long-term health and environmental hazards. Their persistence causes accumulation over time at so-called 'hot spots', locations with continuous increased concentrations of organic fluorine-containing compounds. Intensive purification and regeneration of the land after exposure remains the only option.[5] Also, bioaccumulation occurs during exposure to poly/perfluorinated alkyl substances (PFAS), as nature has not developed a system that addresses the rejection or the digestion of fluorinated carbons.[6] The stability that enhances battery lifetime is preventing natural routes from degrading to environmentally harmless substances. Therefore, the public opinion and legal standpoint on fluorinated compounds, especially the fluorinated polymers (poly/perfluorinatedalkyl substances or PFAS), have shifted from 'highly appreciable' to 'not preferable unless necessary' at best.[7] Within the EU, there is the intention under review to have a restriction on 'the manufacture, placing on the market and use of PFASs'.[8] In the US, similar developments were announced.[9] However, some applications, such as lithium batteries, currently need PFAS for their high performance. If other options exist, they are preferred and should be chosen. Showing alternative chemistries with similar performance during operation is, therefore, instrumental to be able to enforce a PFAS ban in battery applications. Moreover, from a recycling perspective, banning PFAS binders from battery chemistry would enhance the electrode recyclability.[10] Also, the presence of fluorine during recycling, specifically the pyro- and hydrometallurgical processing, complicates the recycling process as well due to the formation of highly corrosive HF.[11] In this context, this perspective focuses on showing a completely fluorine-free battery composition that may replace the current fluorinated ones. Various approaches for fluorine-free battery designs,[12] electrolytes,[13,14] and binders[15,16] have been proposed. Here, such systems are compared, where the fully fluorine-free battery shows high rate performance over a large potential window (2.7-4.3 V) and can cycle more than 500 times with high capacity retention.

2. Fluorine-Free Binder Strategy

The intrinsic advantage of lithium-ion batteries is the high cell potential which stems from the large potential window between anodes at a reduction potentials down to the extreme of Li/Li^+ at −3.04 V versus SHE, and cathode at an oxidation potential which can be as high as +1.46 V versus standard hydrogen electrode (SHE, +4.5 V vs Li/Li^+) for nickel-rich layered oxides. The high oxidation potential at the battery cathode limits the applicability of several polymer binders, especially if potentially oxygen-releasing cathode materials are used; organic binders consisting of unprotected carbon chains may be subject to oxidation from instabilities

M. Weijers, P. Karanth, J. Borninkhof, F. M. Mulder
Department of Chemical Engineering
Faculty of Applied Sciences
Delft University of Technology
Van der Maasweg 9, 2629 HZ Delft, the Netherlands
E-mail: f.m.mulder@tudelft.nl

Supporting information for this article is available on the WWW under https://doi.org/10.1002/batt.202500469

occurring at the active material interfaces.[17] Degradation and potential contact loss of binder to active material lead to a fade in capacity, which would reduce the battery's lifetime. At the anode, this problem is less prominent as it resides at highly reducing potentials around −3.04 V versus SHE. For this reason, F-free organic binders have already been used commercially at the anode.

The second concern is the processability of the binder and active material. For a fluorinated binder like PVDF, organic solvents, such as N-methylpyrrolidone, are used, although they are toxic. Such organic solvents are also used because of the limited compatibility of cathode active materials with more benign solvents like water. In their discharged state, nickel-rich layered oxides are typically prone to exchange of lithium and hydrogen when exposed to water.[18] The effect results in a higher lithium hydroxide concentration and, thereby, a higher alkalinity (higher pH) of the solution. Many studies, however, have addressed this issue, proposing processing methods, which include extensive drying, limited contact times, and/or addition of acids and base components to the solvent.[19–22] As a result, the degradation of cathode active material by water-based processing has been minimized to a marginal difference.[22] The fluorine-free organic binders, which are unlike many fluorinated ones, soluble in water, thus become available. Therefore, an additional advantage beyond the potential phasing out of PFAS is the less harmful processing of these binders in water as a solvent as well.

A list of organic binders, highlighting their applicability and their advantages and disadvantages, is shown in Table S1, Supporting Information. The most promising options for fluorine-free binders have been polyacrylic acid (PAA) and carboxy methyl cellulose combined with styrene butadiene rubbers (CMC/SBR).[21,23,24] Here, the graphite anode and the $LiNi_{0.8}Mn_{0.1}Co_{0.1}O_2$ (NMC811) cathode are produced using PAA and CMC/SBR, respectively. Advantages of using PAA in graphite anodes are their thermal stability and maintained electrolyte accessibility at low porosity, resulting in improved energy densities.[25] For anodes which incorporate silicon in future fluorine-free batteries, to increase the energy density further, PAA or PAA/CMC are the most suitable options as they offer higher cycling stability.[26] Silicon anodes in fluorine-free systems also do not suffer from fluorine-containing decomposition reactions creating HF when combined with the PAA acidic groups, which otherwise would cause silicon dissolution of SiO_x in the solid electrolyte interface (SEI).[27] The choice of CMC/SBR as binder in NMC811 cathodes is based on comparable performances to conventional PVDF binder reported for similar NMC cathodes[23] and the possibility of functionalization to passivate the SEI further.[28,29] This article highlights that combining such organic binders with specifically fluorine-free electrolytes offers advantages considering the SEI stability, leading to a high cycling life.

3. Fluorine-Free Electrolyte

To ensure the electrolyte function, the Li^+ conducting salt needs to have high stability in oxidative and reductive environments to prevent degradation at the cathode and anode respectively. Further, the conductive ion in the salt needs to have limited solvation and binding strength to its counterion to reduce the energy cost of transferring the ion from the bulk electrolyte phase, through the electric double layer to the active material at the electrode interfaces.[30] These combined demands have proved to be challenging.[31] Electrochemical stability often goes hand in hand with the high energy cost of ionic transfer. The development of fluorine-free salts that cover both aspects has been a field of research, which has yielded only a few feasible options so far, as treated by Hernandez et al in previous studies.[31] An asymmetric, charge delocalized counterion with moderate to high ionic strength seems pivotal in generating both charge dissociation in conventional electrolyte solvents, while maintaining low lithium-ion solvation by solvent molecules surrounding the ion pair in the electric double layer of the anode.[31–33] The latter is necessary to reduce side reactions of solvent molecules. Generating a stable SEI composition, with additives or solvent, should then finally minimize side reactivity at the active sites.

One of the most promising options for fluorine-free salts is lithium bis(oxalato)borate (LiBOB).[34,35] LiBOB synthesis is performed using a benign route of wet processing HBO_3 with lithium hydroxide and dioxalic acid.[36] It contains a quaternary oxygenated boron ion, of which the oxygen atoms are linked to ethene to prevent reduction. The ion is fairly large and has been shown to support limited ionic conductivity and has limited solubility in carbonate electrolytes.[37] It is, however, fairly stable at both cathode and anode interfaces after initial interphase formation. LiBOB is also used as an additive, as it decomposes at the anode and cathode resulting in a conducting SEI,[38] CEI,[39] and a passivated aluminum current collector,[40] which may be stabilized together with polymerizing additives like vinylene carbonate (VC) or 1,3,2-dioxathiolane 2,2 dioxide (DTD).[41,42]

Another commonly used salt is $LiNO_3$, which most often functions as a sacrificial salt to increase conductivity in the SEI layer. The potential stability of $LiNO_3$ is not suitable to act as a conducting lithium salt in carbonate electrolytes, as the molecule is preferably reduced.[43] However, by modifying the solvation shell, stable cycling has been demonstrated in LNO:graphite and LFP:graphite cells.[44] The $LiNO_3$ salt shows extraordinary performance in CEI formation for applications in wide temperature ranges,[45] showing conductivity between −60 and 80 °C. Also, in combination with $LiClO_4$, a stable SEI in lithium metal can be formed using $LiNO_3$.[46] In this work, instead of $LiNO_3$ as sacrificial salt, we demonstrate the combination of the passivating behavior of LiBOB combined with VC and DTD, as it is known to passivate the aluminum current collector.

Lithium perchlorate, $LiClO_4$, has been another candidate with widespread attention in the past due to its high ionic conductivity.[47] However, $LiClO_4$ is a strong oxidizing agent, which has a tendency to create oxygen radicals and has shown reactivity with the aluminum current collector above 3.2–3.5 V versus Li/Li^+.[48,49] However, LiBOB is known to passivate the aluminum surface.[50] The use of $LiClO_4$ has caused concerns considering safety and is currently restricted to limited use for practical lithium-ion batteries. The electrolyte solvents used in conventional liquid-state Li-ion batteries are usually flammable, which is also the case here. As these solvents are normally nonfluorinated, this has similar flammability to conventional liquid-state Li-ion batteries. Nevertheless, its use has been compared to $LiPF_6$ by Marom et al.[51] arguing

previous safety experiments were conducted using solely lithium metal anodes, while for graphite, the main conclusion is that "in terms of onset temperatures for thermal runaway, the two electrolytes are equivalent".

4. Comparison of Fluorine-Free Single and Combined Electrolyte Salts

To illustrate the good performance of fluorine-free electrolyte salts, LiBOB is used without and combined with $LiClO_4$ to show 1) the high (electro)chemical stability of fluorine-free battery cells, and 2) an increased lithium conductivity by combining the two salts, which would further bring forward the usage of electrolytes like LiBOB for batteries that need high rate performances. Compared to pure LiBOB, we propose that a salt addition similar to $LiClO_4$ would be necessary to increase the bulk mobility, while LiBOB, VC, and DTD adequately stabilize the interfaces with the electrodes. The comparison shows that a completely fluorine-free battery can have very similar cycling performance to fluorine-containing batteries.

The fluorine-free electrolytes show lower conductivities than generally reported for liquid electrolytes. The ionic conductivity of 0.6 M LiBOB and 0.6 M $LiClO_4$ in EC:dimethyl carbonate (DMC) in blocking conditions in a stainless steel cell configuration shows $\sigma_{SS,RT} = 1.6 \pm 0.3$ mS cm^{-1} and 1.5 ± 0.3 mS cm^{-1}, respectively. The conductivity decreases to $\sigma_{ele,RT} = 0.12$ and 0.07 mS cm^{-1} and $\sigma_{Li,RT} = 0.06$ and/0.04 mS cm^{-1}, respectively, when measured in wetted Celgard 2400 separators in symmetric lithium cells. Such a steep decrease in conductivity when wetted on the separator can be the result of poor compatibility with the separator.[52] Practical conductivity of 0.3 M/0.3 M LiBOB/$LiClO_4$ in symmetric lithium cell, however, increases to $\sigma_{ele,RT} = 0.65$ mS cm^{-1} and $\sigma_{Li,RT} = 0.13$ mS cm^{-1}.

The chemical stability of $LiClO_4$ is a second concern, as reduction of $LiClO_4$ occurs (**Figure 1**C, arrow at 0.7 V), probably to LiCl and Li_2O.[53] LiBOB, however, only shows mild oxidation during the initial sweep (Figure 1B, arrow), after which no additional side reactivity is observed. $LiPF_6$ shows only minor side reactivity above 4.2 V, indicating mild ethylene carbonate (EC) oxidation, becoming larger every sweep (Figure 1A, arrow).

To test the buildup of SEI resistance, electronic impedance spectroscopy (EIS) is carried out before and after a galvanostatic test at 0.1 mA cm^{-2} in symmetric lithium cells for 1 h. An increase in charge transfer resistance can be observed for 0.6 M $LiClO_4$, while for the electrolytes containing LiBOB, this effect remains marginal (Figure 1D, increase in first semicircle). The EIS fitting indicates two semicircles for all fits (fitting results can be found in Table S2, Supporting Information). Typically, the SEI and charge transfer are observed at different characteristic frequencies.

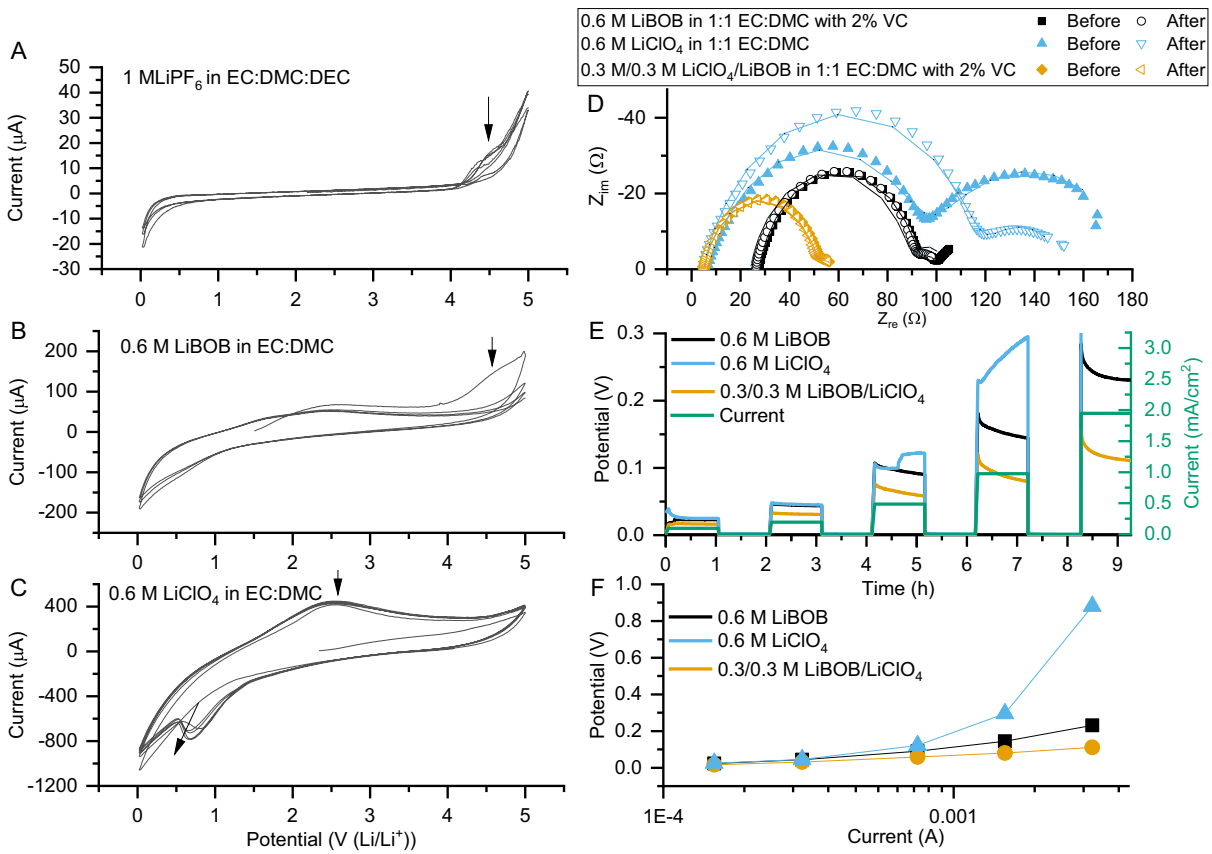

Figure 1. Chemical stability of A) $LiPF_6$, B) LiBOB, and C) $LiClO_4$ lithium salts in carbonate solvents measured using CV at 0.1 V s^{-1} in lithium/aluminum half cells for three sweeps. $LiClO_4$ shows an additional reduction reaction at 1 V (red arrow). D) Nyquist plot of symmetric lithium cells shows increasing SEI resistance with $LiClO_4$ electrolyte, which is reduced when introducing LiBOB salt. E) Step amperometry and F) Tafel plot of end point potentials during step amperometry in symmetric lithium cells show a lower overpotential for the 0.3 M/0.3 M $LiClO_4$ electrolyte as a result.

Perspective
doi.org/10.1002/batt.202500469
Chemistry Europe
European Chemical Societies Publishing

Charge transfer resistance, of which the double layer capacitance in parallel is fitted typically in the microfarad order, shows small resistances for LiBOB-containing species before and after the galvanostatic cycling period. $LiClO_4$ cells, however, show an increase in charge transfer resistance, indicating that slight passivation of the lithium interface may have occurred. SEI resistance shows an increase for the LiBOB-containing cells. The $LiClO_4$ cell here shows a lowered SEI resistance, which indicates the passivation layer is not stable and is renewing constantly. A combination of both salts in an electrolyte may effectively show lower polarization due to elevated ion conductivity, while maintaining a stable interface at the electrode interface. This is illustrated by the step amperometry results in Figure 1E. Here, $LiClO_4$ electrolyte initially shows similar polarization compared to LiBOB, after which it starts to show a buildup of additional polarization after a few hours of galvanostatic current while the polarization of LiBOB and LiBOB/$LiClO_4$ electrolytes maintains fairly Tafel like behavior (Figure 1F), with at most a small ohmic contribution: the DC potential grows much less than linearly with current, indicating that an activated Buttler Volmer type behavior is still dominating the observed overpotential. The deviation from Tafel behavior becomes large, however, for pure $LiClO_4$ electrolyte, indicating a strongly current-dependent resistance term.

5. Fluorine-Free Full Battery, Performance Comparison of Single and Combined Salt Electrolytes

In this work, we report the performance characteristics of a battery containing state-of-the-art graphite anodes and NMC811 cathodes in which PAA and SBR/CMC binders are utilized for anode and cathode, respectively. Using the combined salt configuration, excellent cycling stability and fair rate capabilities at room temperature (RT, 18 °C, **Figure 2**D). We show, however, that there remains a trade-off between stability and rate performance. On one hand, LiBOB shows very high cycling stability (Figure 2C),

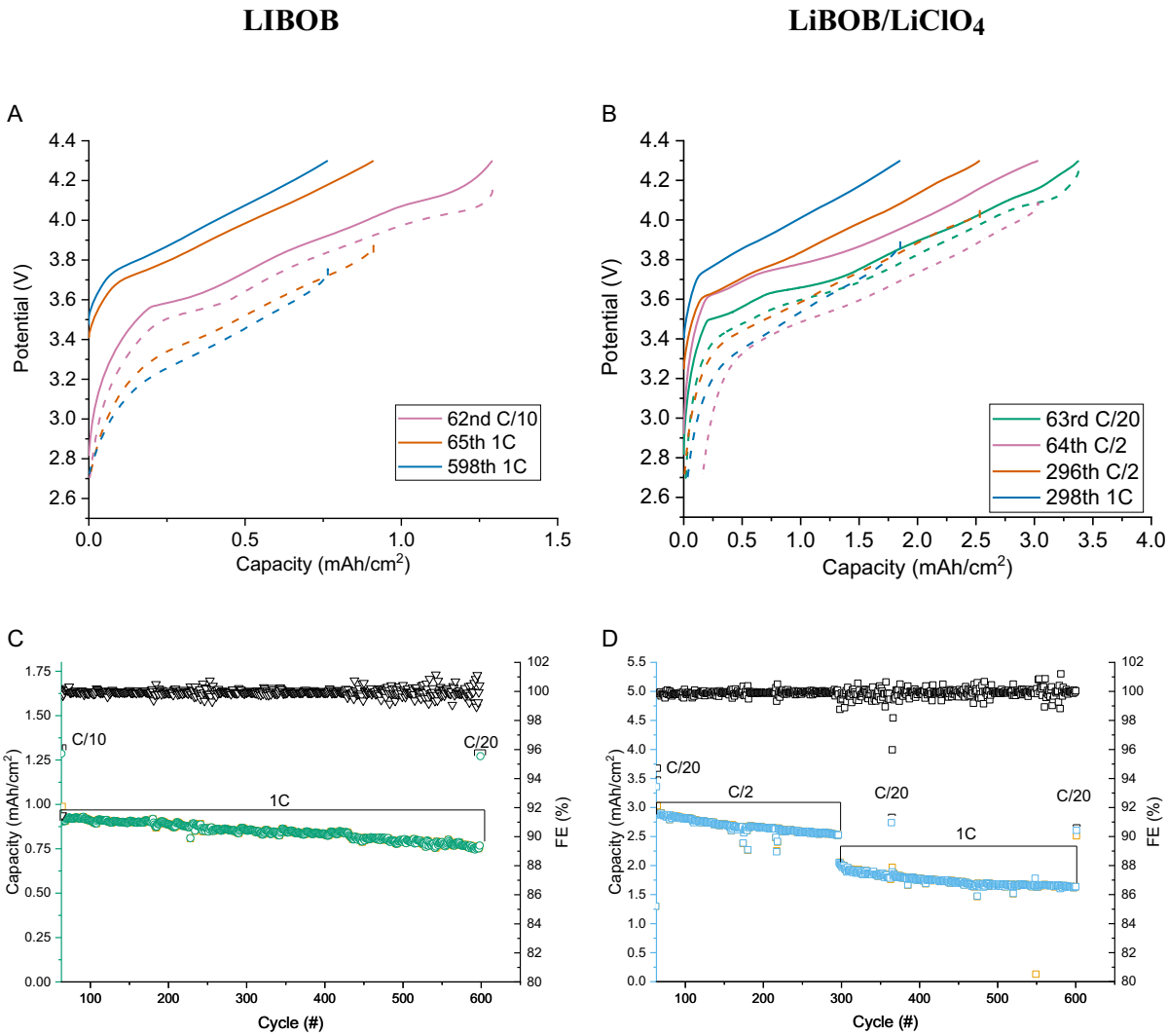

Figure 2. A,B) Potential trace (solid charge, dotted discharge) and C,D) cycling performance of NMC811/graphite full cells. A/C: cell with theoretical areal cathode loading of 1.3 mAh cm^{-2} with 0.6 M LiBOB in 2/49/49 v/v% VC/EC/DMC electrolyte. B/D: same electrode materials but with theoretical areal cathode loading of 3.3 mAh cm^{-2} illustrating the enhanced conductivity of the electrolyte with 0.3/0.3 M LiBOB/$LiClO_4$ in 1/2/48.5/48.5 v/v% DTD/VC/EC/DMC.

which comes at the cost of limited round-trip energy efficiency due to high overpotentials. On the other hand, the combined LiBOB/$LiClO_4$ salt shows excellent rate performance with a slightly lower cycling stability as a trade-off. In Figure 2A, the potential trace during galvanostatic cycling of a LiBOB full cell is shown. At relatively low C/10 (dis)charge rates, a significant potential difference between charging and discharging is already observed at 50% depth of (dis)charge. This mainly originates from the potential drop in the electrolyte caused by its sluggish bulk diffusivity. The LiBOB cell shows a 99 mV potential difference between charge and discharge at C/10 or 0.15 mA cm^{-2}. The energy efficiency of the cell is 95%. A higher current density of 1.5 mA cm^{-2} (1C) shows 460 mV potential difference, yielding 87.4% energy efficiency. At this cycling rate, the capacity retention is reduced to 70.5%. The low electrolyte conductivity contributes heavily to the overpotential, and therefore, capacity fade at higher charge rates. This performance difference in conductivity affects the energy efficiency and allowable electrode loading for achieving fair rate performances. Therefore, a LiBOB/$LiClO_4$ cell is shown with 2.5 times the mass loading to illustrate the beneficial performance of the mixed ion electrolyte.

Upon long-duration cycling, initially, the current density of LiBOB and LiBOB/$LiClO_4$ cells is kept at 0.15 mA cm^{-2} to compare cell overpotentials (Figure S2, Supporting Information), ignoring the contributions of the relatively low double layer resistances at these currents. Then, the C-rate definition is utilized for a longer cycling period (Figure 1C/D). The LiBOB/$LiClO_4$ cell shows a reduced 70 mV potential difference at 0.15 mA cm^{-2} (Figure 1B) with an energy efficiency of 98%. This is 3% more compared to LiBOB and is acceptable for lithium-ion batteries at the cell level.[54] At 1C, the overpotential (483 mV) and capacity retention (66%) are similar to the 1C performance of the LiBOB cell, which contained 2.5 times lower loading. The lower overpotential of LiBOB/$LiClO_4$ allows a higher current, yielding 86.1% energy efficiency at 1C with 7.14 mWh cm^{-2} (and 2.05 mAh cm^{-2}) energy density (which was 3.05 mWh cm^{-2}, 0.9 mAh cm^{-2} for LiBOB at the same C-rate). The difference in rate performance illustrates a route to lower the overpotentials in the electrolyte by the addition of the $LiClO_4$ salt.

In Figure 2C, the cycling results of a LiBOB NMC811/graphite full cell are shown. The LiBOB cell shows 98% retained capacity in the 600th cycle at C/20 (Figure 2C). This shows that the LiBOB cell is able to obtain both anodic and cathodic stability. In contrast, the LiBOB/$LiClO_4$ cell retained 74.8% of its capacity after 600 cycles (Figure 2). In terms of performance loss at 1C, the difference is smaller. During the last 300 1C cycles, the LiBOB/$LiClO_4$ cell loses 18% capacity at 1C, compared to 12% for the LiBOB cell. The apparent stability of the LiBOB cell does not mean there is no change observed when comparing resistances due to electrolyte degradation and SEI buildup, as shown by EIS (**Figure 3** top, fitting results shown in Table S4, Supporting Information). Charge transfer resistances through the SEI and double layer capacitance typically occur between 10 and 1000 Hz[55] and show several Ohms difference (100 Hz arrow). The electrolyte resistances R_{ele} at 100 kHz show only a marginal increase (pristine: 10.7 Ω, cycled: 13.0 Ω). Although these changes occur, they only imply that at higher rates, the voltage cutoff is reached earlier. At C/20, the

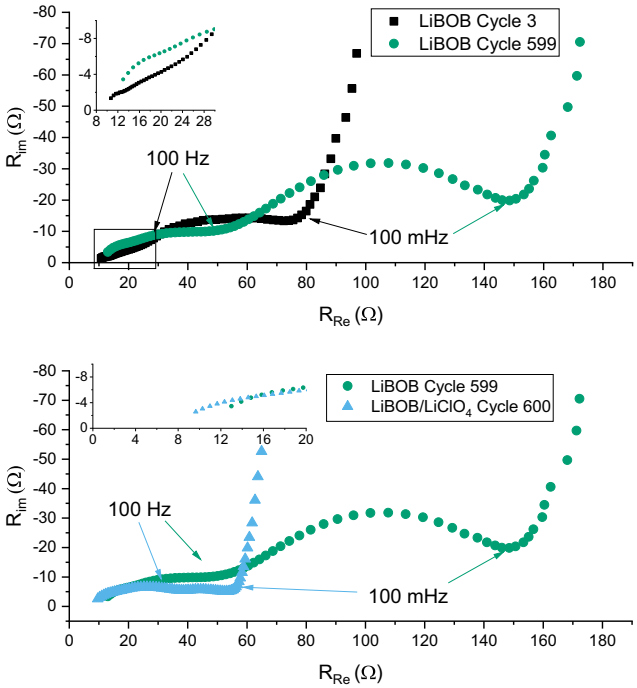

Figure 3. Top) EIS of fluorine-free NMC811/graphite full LiBOB cells at OCP = 2.7 V after formation and extensive cycling. Bottom) EIS spectra of fluorine-free NMC811/graphite full LiBOB and $LiClO_4$ cells after cycling, at 2.7 V OCP. Loading and electrolyte composition between cells differed. LiBOB: 1.3 mAh cm^{-2} with 0.6 M LiBOB in 2/49/49 v/v% VC/EC/DMC, and LiBOB/$LiClO_4$: 3.3 mAh cm^{-2} with 0.3/0.3 M LiBOB/$LiClO_4$ in 1/2/48.5/48.5 v/v% DTD/VC/EC/DMC. High-frequency impedance shows electrolyte resistance R_{ele} (7.8 Ω, 100 kHz) of LiBOB/$LiClO_4$ remains lower compared to LiBOB (pristine: 10.7 Ω, cycled: 13.0 Ω). Lower frequencies are not directly comparable due to differences in cathode and anode loading.

capacity is still accessible, meaning limited Li inventory loss in irreversible SEI formation and/or lithium plating at high charge rates, and thus, limited capacity loss is observed. For the $LiClO_4$ containing electrolyte, it is observed that R_{ele} remains lower after cycling (9.7 Ω) compared to the pristine LiBOB cell (13.0 Ω) (Figure 3, bottom). A large change in capacitive response is observed in the low-frequency impedance range (100 Hz–100 mHz) which may originate from the limited lithium loss in NMC, which makes that the electrode in the fully discharged state (OCP = 2.7 V) is nevertheless different; nonblocking diffusional resistances deeper in the crystallites can extend the low frequency and more resistive response.[56]

6. Composition of the SEI

The formation of a stable SEI on the anode plays a central role in making the long-term cycling of the combination of electrodes and electrolyte in the full cell possible. To observe the resulting SEI in these fluorine-free full cells, they were opened, and graphite electrodes were retrieved. The electrode integrity seems unaltered, and a smooth film layer is formed on both LiBOB and LiBOB/$LiClO_4$ cells (SI Figure S5, Supporting Information). The surface composition of the cell containing LiBOB/$LiClO_4$ shows a slightly lower binding energy for Li1s compared to the LiBOB cell

(0.5 eV, **Figure 4**B and A, respectively), which may originate from a higher abundance of $LiBO_2$ species. The abundance of boron on graphite electrodes after cycling was higher for LiBOB (5.0 +/− 0.5 %at) compared to LiBOB/$LiClO_4$ (3.4 +/− 0.3 at%) cells, as measured with X-ray photoelectron spectroscopy (XPS) (SI Table S4, Supporting Information).

Two clear chemical environments of boron could be identified, of which the LiBOB/$LiClO_4$ cell shows an increased fraction of boron with higher binding energy (32.6% B1s(1)/$B1s_{total}$ in Figure 4C) compared to LiBOB cells (13.5% B1s(1)/$B1s_{total}$; Figure 4D). DTD in the LiBOB/$LiClO_4$ resulted in 1.2 at% sulfur present on the surface. A low amount of chlorine (0.3 at%) is

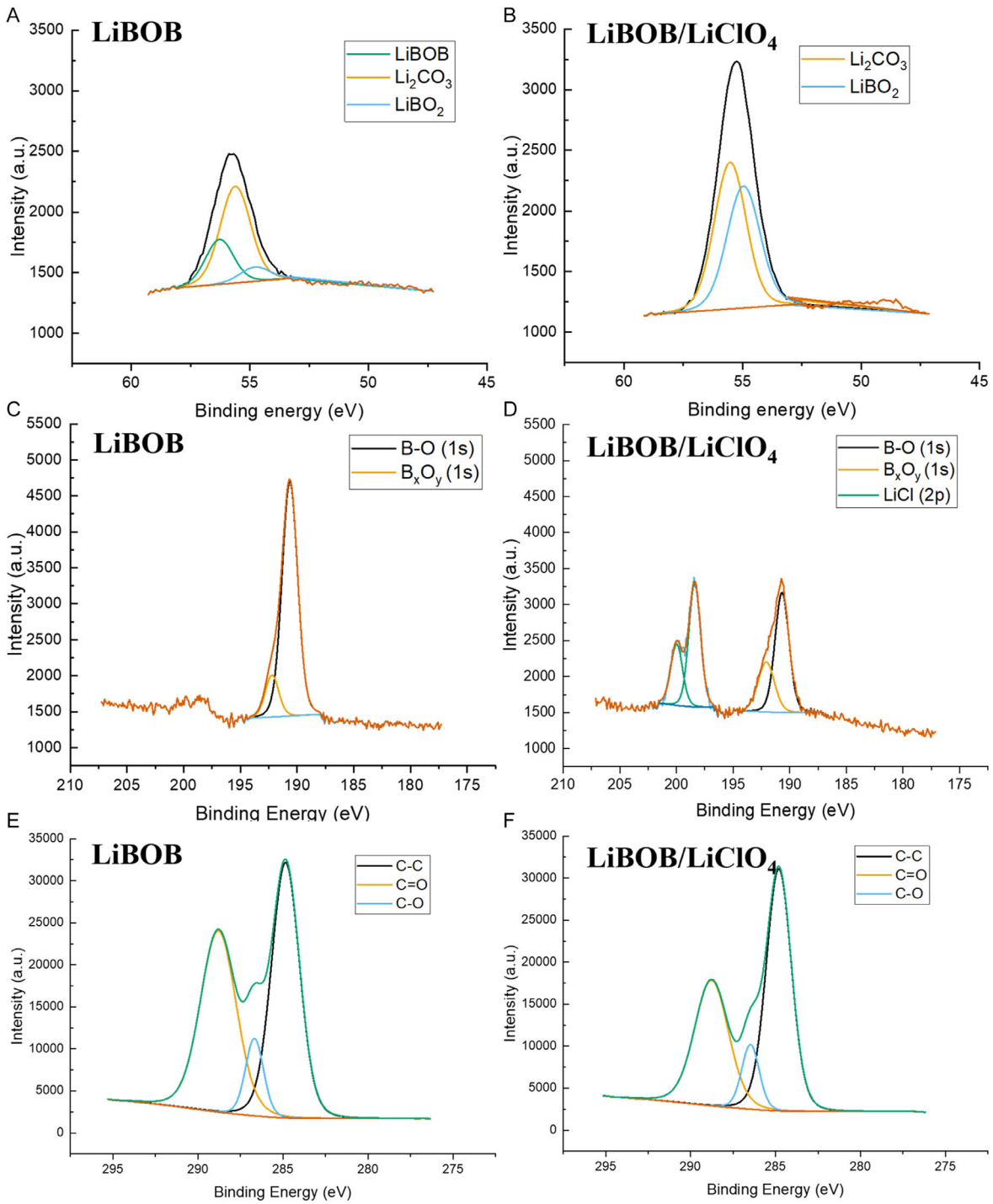

Figure 4. XPS Profile of graphite electrode after cycling. Li1s scan of A) LiBOB and B) LiBOB/$LiClO_4$ indicates a slightly lowered oxidation state of lithium in the SEI upon the presence of $LiClO_4$ in the electrolyte. Allocation of environments according to.[59] Boron B 1*s* and Chloride Cl 2*p* spectrum of C) LiBOB and D) LiBOB/$LiClO_4$ showing a change in oxidation state of boron, which is increased compared to LiBOB. Carbon C 1*s* spectrum of E) LiBOB and F) LiBOB/$LiClO_4$ indicating graphite/hydrocarbon C—C, semicarbonate-like C = O and polyether/carbon C—O species.[38]

observed, indicating a low amount of LiCl or other degradation products from $LiClO_4$ is formed. The LiBOB/$LiClO_4$ shows a higher amount of (semi)carbonate compared to polyether/C—O in the C1*s* spectrum (Figure 4E,F), which is characteristic of LiBOB degradation products in the SEI and in line with the abundance of the Li1s carbonate environment.[38] Polyethers are more typically of polymerization originating from radical reactions, forming CO_2 during EC degradation.[38] The SEI composition, thus, is dominated by carbonates (38 at% and 34 at% C for LiBOB and LiBOB/$LiClO_4$), with boron-containing degradation products from LiBOB (both cells) and sulfur from DTD (LiBOB/$LiClO_4$ cell). Both are known for their good SEI stabilization performance. Although the oxidation state of boron species shows a slightly higher abundance for LiBOB/$LiClO_4$, no major change in organic/inorganic SEI composition is observed between LiBOB and LiBOB/$LiClO_4$ cells.

7. Conclusion

The fluorine-free LiBOB/PAA/SBR/CMC-based battery shows outstanding capacity retention, while not using a fluorine-based materials inventory. This illustrates that the use of fluorine can be prevented while maintaining battery stability. $LiClO_4$ addition to the electrolyte yields improved rate performances at higher areal capacities, at the cost of increased capacity fade during long-term cycling. For higher areal capacity batteries, the addition of $LiClO_4$ may be considered, as it increases the ionic conductivity, and with respect to safety, the thermal instability onset is reported to be similar to that of $LiPF_6$.[51]

The graphite electrode structure after cycling is unaltered, as observed by scanning electron microscopy (SEM). Also, the SEI composition for LiBOB/$LiClO_4$ seems to be improved when compared to LiBOB. The LiBOB cell contains a lower abundance of (stable) LiBOB degradation products compared to LiBOB/$LiClO_4$. The abundance of chlorine (from $LiClO_4$) on the surface is relatively low, indicating low amounts of LiCl formed.

These results highlight that fluorine-free lithium-ion batteries are achievable in batteries with realistic areal capacities using the appropriate fluorine-free binders and a fluorine-free electrolyte salt. Acceptable (dis)charge rates and durability are observed, compatible with typical applications where (dis)charge rates of C/2 – 1C with active mass loadings greater than 1.5 to 3 mAh cm^{-2} are required. Such battery-powered applications include laptops, power tools, and electric vehicles,[57,58] therefore, enabling the electrification of various sectors, reducing their fuel-related CO_2 emissions. As fluorine chemistry can now also be omitted, the related PFAS emissions during battery manufacturing and recycling can be prevented as well, further lowering ecological footprints in battery-enabled electrification.

8. Experimental Section

Graphite anodes were made using 90/5/5 m/m% Timrex E-SLS 30 graphite (Imerys)/PAA binder (3000 K, Aldrich)/carbon Super P C45 (MSE). The powder mixture was suspended in three steps using a top stirrer (IKA). First, 18:1 water-to-powder mass was added to a container, and after initially suspending for 15 min, a 2:1 water-to-powder mass ratio was added. This was repeated a second time until a castable slurry was obtained. A coating was made using a 200 and 300 μm doctor blade casting on copper foil, after which the coating was dried in a vacuum oven at 60 °C for at least 16 h.

NMC811 cathodes were made using 94/3/1/1 m/m% NMC811 (Gelon, polycrystalline)/carbon Super P C45 (MSE)/KS4 (Timcal)/SBR (15 wt% stabilized suspension, Targray)/CMC (Sigma). Powders were suspended in a 12:1 water-to-powder ratio. An ink was obtained after 60 min. A coating was made using a 150 and 250 μm doctor blade casting on aluminum foil, after which the coating was dried in a vacuum oven at 60 °C for at least 16 h and subsequently for 16 h at 80 °C.

Dried anode and cathodes were punched into 14 and 15 mm diameter circles, respectively, and subsequently assembled in a CR2032 coin cell using a Celgard 2400 separator with 90 μl electrolyte. The base LiBOB electrolyte used is 0.6 M LiBOB in 2/49/49 v/v% VC/EC/DMC (E-lyte). A second electrolyte with increased conductivity and stabilizing agent DTD (Merck Sigma) was formulated as 0.3/0.3 M LiBOB/$LiClO_4$ in 1/2/48.5/48.5 v/v% DTD/VC/EC/DMC, called LiBOB/$LiClO_4$. A reference electrolyte of 1 M $LiPF_6$ in 1/1/1 v/v/v% EC/DMC/DEC (Merck Sigma) was used during the chemical stability tests.

Galvanostatic cycling was performed after a 24 h rest period on a MACCOR-4000 cell cycler between 2.7 and 4.3 V. Fast discharging was tested initially at C/10 charge rate and C/10, C/5, C/2, and 1C discharge rate for five discharge cycles each. After the rate performance for cycling again, a period of 40–42 cycles at C/10 charge and discharge rate was used. After this period, 1C charge and discharge rates cycling was initiated. For LiBOB/$LiClO_4$ cells, initially, the same current density for the same set period was used to compare electrolyte aging, meaning the tests were performed at 0.4 times the C-rate indicated above, after which the full potential window and appropriate C-rate were used to test the cell performance further. EIS, cyclic voltammetry (CV), potentiostatic intermittent titration (PITT), and step amperometry were measured on a Parstat MC200 Module. EIS was measured at 2.7 V between 100 kHz and 10 mHz AC frequencies at 10 mV amplitude. Chemical stability was measured using CV at a scan rate of 0.1 V s^{-1} from OCP in the potential range of 0–5 V in Li/Al cells, using a glass fiber separator immersed with electrolyte. Electrolyte conductivity was measured using two stainless steel plates with a polypropylene spacer of 47 μm with a 10 mm diameter hole filled with electrolyte using EIS. Step amperometry and PITT (dU = 0.01 V) were measured in symmetric lithium metal cells with Celgard 2400 as a separator in C2032 coin cells. Conductivity values were calculated by using Equation (1), taking PITT steady state current I_{ss}, charge transfer resistance R_{ct}, and electrolyte resistance R_{ele} (Table S2, Supporting Information). The cell area A, if applicable Celgard porosity ε (40%) and thickness (25 μm) were used.

$$\sigma = \frac{d}{A * \varepsilon * (R_{ss} - R_{ct})} \quad (1)$$

To perform postmortem analyses, graphite electrodes were retrieved from coin cells after cycling. The samples were washed with DMC to remove salt traces and dried. SEM images were taken using a JSM-IT700HR FE-SEM setup (JEOL) in scattering electron imaging (Acc. Voltage: 1 kV - 5 kV). Energy-dispersive X-ray spectroscopy was performed in Backscattered electron composition (Acc. voltage: 20 kV) mode. Surface composition was measured with XPS using a Kα spectrometer (Thermo Fisher Scientific) with an Al Kα source with a spot size of 400 μm. Charge correction was performed by calibrating the adventitious carbon peak (285 eV). For peak fitting, U2 Tougaard background was used.

Acknowledgements

This project has received funding from the European Union's Horizon 2020 research and innovation programme under grant

agreement no. 875557. Neither the European Commission nor any person acting on behalf of the Commission is responsible for how the following information is used. The views expressed in this publication are the sole responsibility of the authors and do not necessarily reflect the views of the European Commission.

Conflict of Interest

The authors declare no conflict of interest.

Keywords: batteries · fluorine-free · lithium · organic binders · organic electrolytes

[1] J. Piątek, S. Afyon, T. M. Budnyak, S. Budnyk, M. H. Sipponen, A. Slabon, *Adv. Energy Mater.* **2021**, *11*, 2003456.
[2] M. Li, J. Lu, Z. Chen, K. Amine, *Adv. Mater.* **2018**, *30*, 1800561.
[3] N. Xu, J. Shi, G. Liu, X. Yang, J. Zheng, Z. Zhang, Y. Yang, *J. Power Sources Adv.* **2021**, *7*, 100043.
[4] Y. Wang, Z. Wu, F. M. Azad, Y. Zhu, L. Wang, C. J. Hawker, A. K. Whittaker, M. Forsyth, C. Zhang, *Nat. Rev. Mater.* **2023**, *9*, 119.
[5] P. Wang, T. Wang, J. P. Giesy, Y. Lu, *Chemosphere* **2013**, *91*, 751.
[6] A. J. Lewis, X. Yun, D. E. Spooner, M. J. Kurz, E. R. McKenzie, C. M. Sales, *Sci. Total Environ.* **2022**, *822*, 153561.
[7] L. R. Dorrance, S. Kellogg, A. H. Love, *Environ. Claims J.* **2017**, *29*, 290.
[8] Per- and Polyfluoroalkyl Substances (PFAS). https://echa.europa.eu/registry-of-restriction-intentions/-/dislist/details/0b0236e18663449b.
[9] EPA, press office. Biden-Harris Administration Finalizes First-Ever National Drinking Water Standard to Protect 100M People from PFAS Pollution. EPA.
[10] A. Wolf, F. Nagler, P. Daubinger, C. Neef, K. Mandel, A. Flegler, G. A. Giffin, *Energy Environ. Sci.* **2024**, *17*, 8529.
[11] M. Wang, K. Liu, J. Yu, Q. Zhang, Y. Zhang, M. Valix, D. C. W. Tsang, *Glob. Chall.* **2023**, *7*, 2200237.
[12] E. K. Savvidou, A. Rensmo, J. P. Benskin, S. Schellenberger, X. Hu, M. Weil, I. T. Cousins, *Environ. Sci. Technol.* **2024**, *58*, 21908.
[13] S. Nam, H. Seong, Y. Kim, K. Kim, C. Kim, S. Kwon, S. Park, *Chem. Eng. J.* **2024**, *497*, 154790.
[14] S. L. Ramesh, J. Lopez, *ACS Energy Lett.* **2025**, *10*, 1671.
[15] J. Jang, J. Ahn, J. Ahn, U. Jeong, J. Yoon, J. K. Park, W. Shin, M. J. Kang, M. Cho, D. J. Kang, J. Kim, J. Yoo, H. Im, *Adv Funct Mater.* **2024**, *34*, 2410866.
[16] F. Leibetseder, J. Xie, E. Leeb, G. Hesser, K. Pettinger, K. Bretterbauer, *Adv. Energy Mater.* **2024**, *14*, 2401074.
[17] T. Dong, P. Mu, S. Zhang, H. Zhang, W. Liu, G. Cui, *Electrochem. Energ. Rev.* **2021**, *4*, 545.
[18] D. Bresser, D. Buchholz, A. Moretti, A. Varzi, S. Passerini, *Energy Environ. Sci.* **2018**, *11*, 3096.
[19] J.-H. Kuo, C.-C. Li, *J. Electrochem. Soc.* **2020**, *167*, 100504.
[20] S. Pedaballi, C.-C. Li, *J. Power Sources* **2020**, *472*, 228552.
[21] S. Radloff, R.-G. Scurtu, M. Hölzle, M. Wohlfahrt-Mehrens, *J. Electrochem. Soc.* **2021**, *168*, 100506.
[22] W. Bauer, F. A. Çetinel, M. Müller, U. Kaufmann, *Electrochim. Acta* **2019**, *317*, 112.
[23] R. Demiryürek, N. Gürbüz, G. Hatipoglu, M. Er, H. Malkoc, O. Guleryuz, G. Uyar, D. Uzun, M. N. Ateş, *Intl. J. Energy Res.* **2021**, *45*, 21182.
[24] B. Boz, M. Vuksanovic, L. Neidhart, M. Höchtl, K. Fröhlich, M. Jahn, *Meet. Abstr* **2022**, *MA2022-02*, 2542.
[25] Y.-S. Park, E.-S. Oh, S.-M. Lee, *J. Power Sources* **2014**, *248*, 1191.
[26] P. Parikh, M. Sina, A. Banerjee, X. Wang, M. S. D'Souza, J.-M. Doux, E. A. Wu, O. Y. Trieu, Y. Gong, Q. Zhou, K. Snyder, Y. S. Meng, *Chem. Mater.* **2019**, *31*, 2535.
[27] C. C. Nguyen, T. Yoon, D. M. Seo, P. Guduru, B. L. Lucht, *ACS Appl. Mater. Interfaces* **2016**, *8*, 12211.
[28] H. Isozumi, K. Kubota, R. Tatara, T. Horiba, K. Hida, T. Matsuyama, S. Yasuno, S. Komaba, *ACS Appl. Energy Mater.* **2020**, *3*, 7978.
[29] A. C. Rolandi, A. Barquero, C. Pozo-Gonzalo, I. De Meatza, N. Casado, M. Forsyth, J. R. Leiza, D. Mecerreyes, *ACS Appl. Polym. Mater.* **2024**, *6*, 1236.
[30] X. Chen, Q. Zhang, *Acc. Chem. Res.* **2020**, *53*, 1992.
[31] G. Hernández, R. Mogensen, R. Younesi, J. Mindemark, *Batteries Supercaps* **2022**, *5*, e202100373.
[32] O. Borodin, *Curr. Opin. Electrochem.* **2019**, *13*, 86.
[33] G. I. Guerrero-García, *Biophys. Chem.* **2022**, *282*, 106747.
[34] W. Song, J. Harlow, E. Logan, H. Hebecker, M. Coon, L. Molino, M. Johnson, J. Dahn, M. Metzger, *J. Electrochem. Soc.* **2021**, *168*, 090503.
[35] K. Xu, S. Zhang, U. Lee, J. Allen, R. Joww, *J. Power Sources* **2005**, *146*, 79.
[36] T. Lestariningsih, Q. Sabrina, I. Nuroniah, B. Prihandoko, E. Marti Wigayati, C. Rina Ratri, *J. Phys.: Conf. Ser.* **2019**, *1282*, 012044.
[37] K. Xu, *J. Electrochem. Soc.* **2008**, *155*, A733.
[38] K. Xu, U. Lee, S. Zhang, M. Wood, T. R. Jow, *Electrochem. Solid-State Lett.* **2003**, *6*, A144.
[39] Y. Dong, B. T. Young, Y. Zhang, T. Yoon, D. R. Heskett, Y. Hu, B. L. Lucht, *ACS Appl. Mater. Interfaces* **2017**, *9*, 20467.
[40] K. Xu, S. Zhang, T. R. Jow, W. Xu, C. A. Angell, *Electrochem. Solid-State Lett.* **2002**, *5*, A26.
[41] J. E. Harlow, X. Ma, J. Li, E. Logan, Y. Liu, N. Zhang, L. Ma, S. L. Glazier, M. M. E. Cormier, M. Genovese, S. Buteau, A. Cameron, J. E. Stark, J. R. Dahn, *J. Electrochem. Soc.* **2019**, *166*, A3031.
[42] J. Li, H. Li, W. Stone, S. Glazier, J. R. Dahn, *J. Electrochem. Soc.* **2018**, *165*, A626.
[43] Y. Quan, X. Cui, L. Hu, Y. Kong, X. Zhang, H. Liang, Y. Zhu, C. Wang, N. Zhang, S. Li, *Carbon Neutralization* **2025**, *4*, e184.
[44] H. Chen, K. Chen, L. Luo, X. Liu, Z. Wang, A. Zhao, H. Li, X. Ai, Y. Fang, Y. Cao, *Angew. Chem. Int. Ed.* **2024**, *63*, e202316966.
[45] S. Yuan, S. Cao, X. Chen, J. Wei, Z. Lv, H. Xia, L. Chen, R. B. F. Ng, F. L. Tan, H. Li, X. J. Loh, S. Li, X. Feng, X. Chen, *J. Am. Chem. Soc.* **2025**, *147*, 4089.
[46] S. Xu, S. Xu, X. Guo, J. Xiong, Z. Wei, S. Zhu, J. Xu, S. Gong, P. Shi, S. Guo, Y. Min, *Adv Funct Mater.* **2025**, *35*, 2500335.
[47] V. Aravindan, J. Gnanaraj, S. Madhavi, H. Liu, *Chem. A European J* **2011**, *17*, 14326.
[48] P. Suresh, A. K. Shukla, S. A. Shivashankar, N. Munichandraiah, *J. Power Sources* **2002**, *110*, 11.
[49] S. S. Zhang, T. R. Jow, *J. Power Sources* **2002**, *109*, 458.
[50] A. Hofmann, M. Schulz, V. Winkler, T. Hanemann, *J. Electrochem. Soc.* **2014**, *161*, A431.
[51] R. Marom, O. Haik, A, D. urbach, I. C. Halalay, *J. Electrochem. Soc.* **2010**, *157*, A972.
[52] H. Yang, X. Shi, S. Chu, Z. Shao, Y. Wang, *Adv. Sci.* **2021**, *8*, 2003096.
[53] X. Fu, X. Deng, Y. Deng, X. Xiong, Y. Zheng, Z. Zhang, D. Dang, G. Wang, *Energy Fuels* **2022**, *36*, 11219.
[54] P. Meister, H. Jia, J. Li, R. Kloepsch, M. Winter, T. Placke, *Chem. Mater.* **2016**, *28*, 7203.
[55] J.-M. Atebamba, J. Moskon, S. Pejovnik, M. Gaberscek, *J. Electrochem. Soc.* **2010**, *157*, A1218.
[56] H. Xiao, Z. Tao, H. Bai, H. Wang, Y. Fu, N. Si, H. Bai, *IOP Conf. Ser.: Earth Environ. Sci.* **2020**, *474*, 052038.
[57] Y. Liu, Y. Zhu, Y. Cui, *Nat Energy* **2019**, *4*, 540.
[58] G. Hernández, A. J. Naylor, Y.-C. Chien, D. Brandell, J. Mindemark, K. Edström, *ACS Sustainable Chem. Eng.* **2020**, *8*, 10041.
[59] Justin Gorham. NIST X-Ray Photoelectron Spectroscopy Database - SRD 20, **2012**, https://doi.org/10.18434/T4T88K.

Manuscript received: June 18, 2025
Revised manuscript received: July 8, 2025
Version of record online: